

Plasmonic enhancement of blue emission from ZnO nanorods grown on the anodic aluminum oxide (AAO) template

Małgorzata Norek · Grzegorz Łuka ·
Marek Godlewski · Tomasz Płociński ·
Marta Michalska-Domańska · Wojciech J. Stępniewski

Received: 8 August 2012 / Accepted: 20 November 2012 / Published online: 1 December 2012
© The Author(s) 2012. This article is published with open access at Springerlink.com

Abstract Luminescent properties of ZnO nanorods covered with Ag nanoparticles are examined. Nanorods were synthesized on AAO templates using Atomic Layer Deposition (ALD) technique. Two types of the samples were prepared with different arrangement of ZnO nanorods and doping conditions. Nanorods of the second type were codoped with Al, to stimulate defect-related emissions. The ZnO material fills heterogeneously the interior of the AAO nanopores and has hexagonal, wurtzite structure. Both types of structures exhibit a broad defect-related emission at about 440 nm, most probably related to recombination at zinc interstitial (Zn_i) defects. This emission in samples with a random distribution of ZnO:Al nanorods and finer Ag nanoparticles is enhanced by factor of ~ 2.5 upon Ag deposition. The so-obtained material is interesting from the point of view of its application in blue range emitting diodes.

1 Introduction

ZnO at conventional growth conditions crystallizes into hexagonal wurtzite structure with the fourfold tetrahedral coordination [1]. Its nanostructures (nanoparticles,

nanorods) are intensively studied due to their possible applications in highly sensitive sensors, as fluorescence labels, photovoltaic materials, etc. [2]. Moreover, 3.37 eV energy band gap of ZnO and high exciton binding energy of 60 meV make ZnO attractive for applications in light-emitting diodes (LED) and in laser diodes (LD) if p-type doping will be mastered.

ZnO, in addition to ultraviolet UV emission being due to free and bound exciton recombination, often exhibits broad band emissions of the donor-acceptor-pair (DAP) origin, associated with the presence of intrinsic or extrinsic defects. Regarding intrinsic defects, oxygen vacancies (V_O), oxygen interstitial (O_i), zinc vacancies (V_{Zn}), zinc interstitial (Zn_i), oxygen anti-site (O_{Zn}), and zinc anti-site (Zn_O) are considered [3, 4]. The extrinsic defects, such as Al, Na, or Li, are also suggested to be involved in deep-level emissions in ZnO [5]. The presence of these defects affects also the electrical properties of the material. For example, ZnO:Al shows metallic conductivity and high optical transparency, making this material suitable for application as transparent contacts [6].

The latter means that ZnO can be used to enhance light emission from GaN-based LEDs, when used as transparent contact [7], and also, when in contact area, part of short-wavelength emission is converted to visible one, as material in so-called hybrid white-light-emitting diodes.

The density of the structures and their surface area are important in point of view of the above-mentioned applications [8]. The smooth surface morphology with well-ordered grains results in the reduction of the intrinsic defects and improvement of efficiency of band-edge emission in UV [9]. In contrary, the rough surface and large surface-to-volume ratio of ZnO nanostructures results in high doping levels. For example, an increased concentration of oxygen vacan-

M. Norek (✉) · M. Michalska-Domańska · W.J. Stępniewski
Faculty of Advanced Technologies and Chemistry, Military
University of Technology, 2 Kaliskiego Str., 00-908 Warsaw,
Poland
e-mail: mnorek@wat.edu.pl

G. Łuka · M. Godlewski
Institute of Physics, Polish Academy of Sciences, al. Lotników
32/46, 02-668 Warsaw, Poland

T. Płociński
Faculty of Materials Science and Engineering, Warsaw University
of Technology, 141 Wołoska Str., 02-507 Warsaw, Poland

cies results in a brighter green emission of ZnO. Band-edge emission in UV spectral region is then weaker [10].

There are several methods to deposit ZnO nanorods [11]. Recently, ZnO nanorods were synthesized using anodic aluminum oxide template (AAO) as a substrate [12–14]. The so-obtained ZnO nanostructures exhibited a broad blue/green light emission, which was ascribed to recombination of carriers trapped at oxygen and zinc vacancies [15, 16]. Importantly, photoluminescence (PL) enhancement was reported for ZnO nanorods deposited on AAO templates. This enhancement was related to the generation of oxygen vacancies at interfaces between ZnO nanorods and pore walls of the AAO [17]. Moreover, strong blue emission was also observed for ZnO nanoparticles embedded in the AAO template and also for ZnO thin films deposited on the AAO. The latter PL emission was ascribed to the increase concentration of Zn interstitials (Zn_i) in the ZnO in the pores of AAO template [18, 19].

PL intensity can be further enhanced by coupling with plasmons in metal nanoparticles. However, in the latter case, not only enhancement, but also quenching can be observed, depending on many factors. The most important is energy matching between PL emission and surface plasmons generated in metal nanoparticles. The particles size, the separation distance between semiconductor and metal, and the surface roughness of metal are also important [20, 21].

Several mechanisms were proposed to account for the plasmonic PL enhancement. The enhancement of UV PL was attributed to the resonant coupling between excitons and surface plasmons (SP) of metal, but also to the increase of the local electric fields induced by localized surface plasmons (LSP) [22, 23]. In turn, the enhancement of the DAP emission was related to the LSP-DAP dipole–dipole scattering [24].

For ZnO nanocrystals, synthesized by sonochemical method, enhancement of blue emission was induced by Ag in the ZnO nanospheres with an average size of about 440 nm [25–27]. This observation motivated the present study. In the present work we deposited ZnO nanorods on the AAO template by the Atomic Layer Deposition (ALD) method. We examine the influence of Ag nanoparticles on the PL properties of deposited ZnO nanorods. Two types of the samples are studied, characterized by different level of the nanorods arrangement and ZnO doping. First type of ZnO nanorods were deposited at 200 °C temperature. ZnO nanorods of the second type were doped with Al [6] and were deposited at reduced temperature of 130 °C. These nanorods were less ordered.

2 Experimental

The AAO template with nanopores of approximately 63.7 ± 4.1 nm in diameter and the inter-pore distance of $93.3 \pm$

1.4 nm was fabricated using two-step anodization method. High-purity 0.25-mm-thick aluminum foil (99.9995 %) was purchased from Alfa-Aesar. The foil was cut into specimens 0.5×2.5 cm. The specimens were degreased in acetone and ethanol. Samples were electropolished in a 1:4 mixture of 60 % perchloric acid and ethanol at constant current density of 0.5 A cm^{-2} . The temperature was kept at 283 K, and the duration of electropolishing was 1 min. As prepared aluminum specimens were coated with acid resistant dye to obtain 0.5 cm^2 of working surface area per sample. Nanoporous alumina was formed by two-step self-organized anodization under 40.0 V cell voltage in a 0.3 M oxalic acid solution at 308 K. To preserve constant temperature, the processes were carried out in double-walled electrochemical cell (0.5 dm^3) equipped with a circulator bath (Lauda 105). The solution was stirred during the anodization. Platinum grid with the surface area of 6 cm^2 was used as a counter electrode. Distance between the platinum grid and anodized aluminum was 3 cm. After the first step of anodization, formed alumina was removed by chemical etching in a vigorously stirred mixture of 6 wt% H_3PO_4 and 1.8 wt% H_2CrO_4 at 333 K. After oxide removal the samples were reanodized at the same conditions as presented in the first step of the process, but the duration of the second step was 7 h and 5 min to obtain 200- μm -thick AAO template.

The ZnO material was deposited on the AAO by the ALD technique. Zinc oxide was grown using organic zinc precursor from diethylzinc (DEZ) and water vapor as oxygen precursors. Trimethylaluminum (TMA) was used for doping with approximately 3 % of aluminum (structures of the second type). The films were grown in Savannah-100 ALD reactor (Cambridge NanoTech). The process pressure was 10^{-1} mbar, and the N_2 purging gas flow rate was 20 sccm. The growth temperature was 200 °C for ZnO nanorods (sample 1) and 130 °C for ZnO:Al (sample 2). Further details on uniform ZnO:Al films can be found in our recent publication [28].

The Ag nanoparticles were deposited on the top of as prepared samples by vacuum evaporation technique at room temperature and under high vacuum of 10^{-6} kPa. All evaporation processes were done using resistively heated tungsten crucibles. After the Ag deposition the samples will be further denoted in the text as samples 1' and 2', respectively.

The luminescence spectra with an excitation wavelength of 300 nm and decay times were measured by Fluorolog-3 spectrofluorimeter (Horiba Jobin Ivon).

The morphology of the investigated samples were examined with a high-resolution field emission scanning electron microscope (FEI, Quanta 3D FEG), equipped with a backscattered electron detector (BSE) and energy dispersive X-ray spectrometer (EDS) and a duo-STEM bright/dark field (BF/DF) detector.

The microstructure of the samples was analyzed with a high-resolution scanning-transmission electron microscope

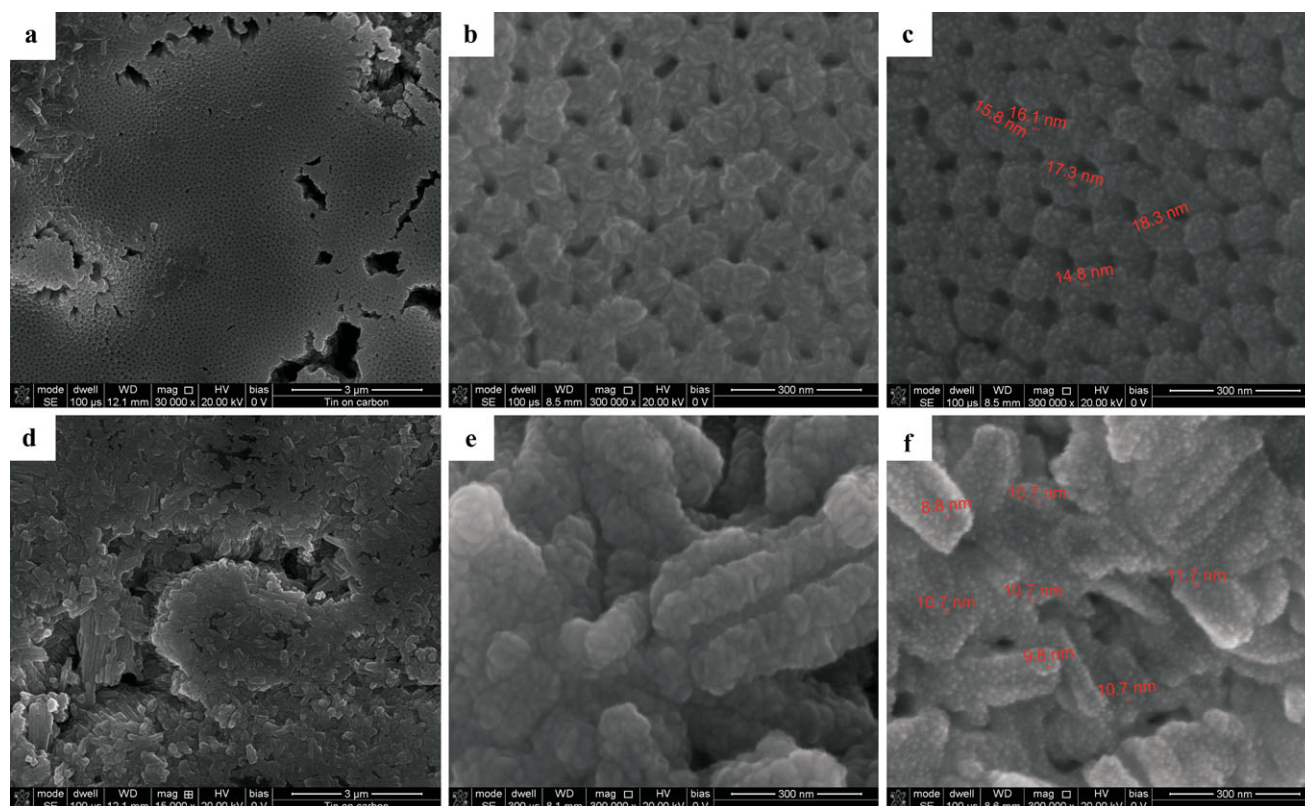


Fig. 1 SEM micrographs of sample 1 (a, b) and 1' (c) and sample 2 (d, e) and 2' (f)

(STEM; Hitachi HD2700) with an accelerating voltage of 200 kV, equipped with the SE/BF/HAADF (High Angle Annular Dark Field), EDS, and an electron energy loss spectrometer (EELS) detectors. Thin foils for electron microscopy were prepared by the focused ion beam (FIB) technique using the FB-2100 Hitachi system. A liquid ion metal source was used as the source of the gallium ion beam. The accelerating voltage used was 40 kV. Tungsten was used as a protective layer. The EDX analysis on crosssection were done by using dual beam system Hitachi NB5000 equipped with ThermoNoran EDX spectrometer.

3 Results and discussion

Figure 1 presents SEM micrographs of the surface of the AAO/ZnO and AAO/ZnO/Ag composite samples. A prominent difference in morphology between samples of the 1st and 2nd type can be observed. The arrangement of the ZnO nanorods in samples 1 is much more regular than in samples 2 (compare Figs. 1a and b with 1d and e, respectively) grown at lower temperature. A hexagonal arrangement, inherited from the AAO substrate, can be detected in the samples 1, whereas in the samples 2 the ZnO nanorods are randomly distributed. The nanorods in both samples seem to have the same diameter and are consisted of tiny, elongated

crystallites of around 60 nm in length. Figures 1c and 1f demonstrate the samples after deposition of Ag nanoparticles. It can be noticed that the Ag nanoparticles have a narrow size distribution between 15–18 nm in samples of the first type and between 9–12 nm in samples of the second type.

Figures 2a and 2b show EDS analysis of samples 1' and 2' (structures of the first and second type covered with Ag particles) confirming the presence of Zn, O, Al, and Ag elements. Al peak partly comes from the template. This is why it is observed both for undoped and Al-doped structures. The Ag lines are very weak because of much lower X-ray emission probability of L-lines compared to K-lines of Zn, Al, or O. Furthermore, the presence of Ag is limited to the surface where the interaction volume is actually determined by the electron probe diameter (the beam spreading is negligible). Since the interaction volume is small, the X-ray signal will be also small for Ag element.

Figure 3 shows BSE micrograph (Fig. 3a) and EDS elemental map of Zn (Fig. 3b), Al (Fig. 3c), and O (Fig. 3d) of the material, respectively, revealing the presence of ZnO in the interior of the AAO nanopores. The ZnO fills the nanopores rather heterogeneously down to approximately 7–8 μm.

The microstructure of sample 1 was analyzed by STEM in more detail. Figure 4 shows scanning electron micro-

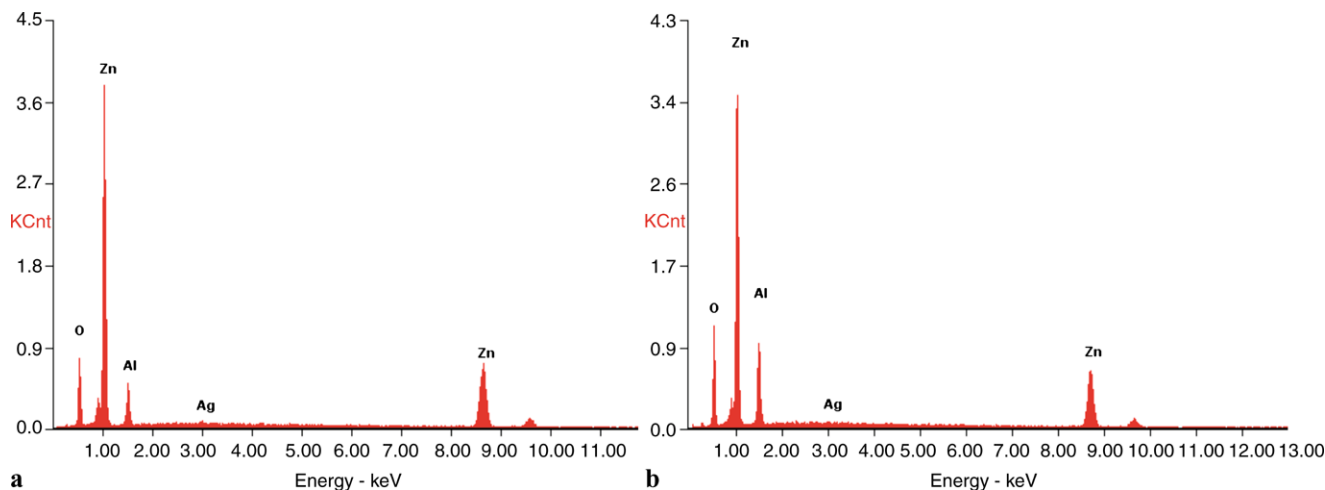
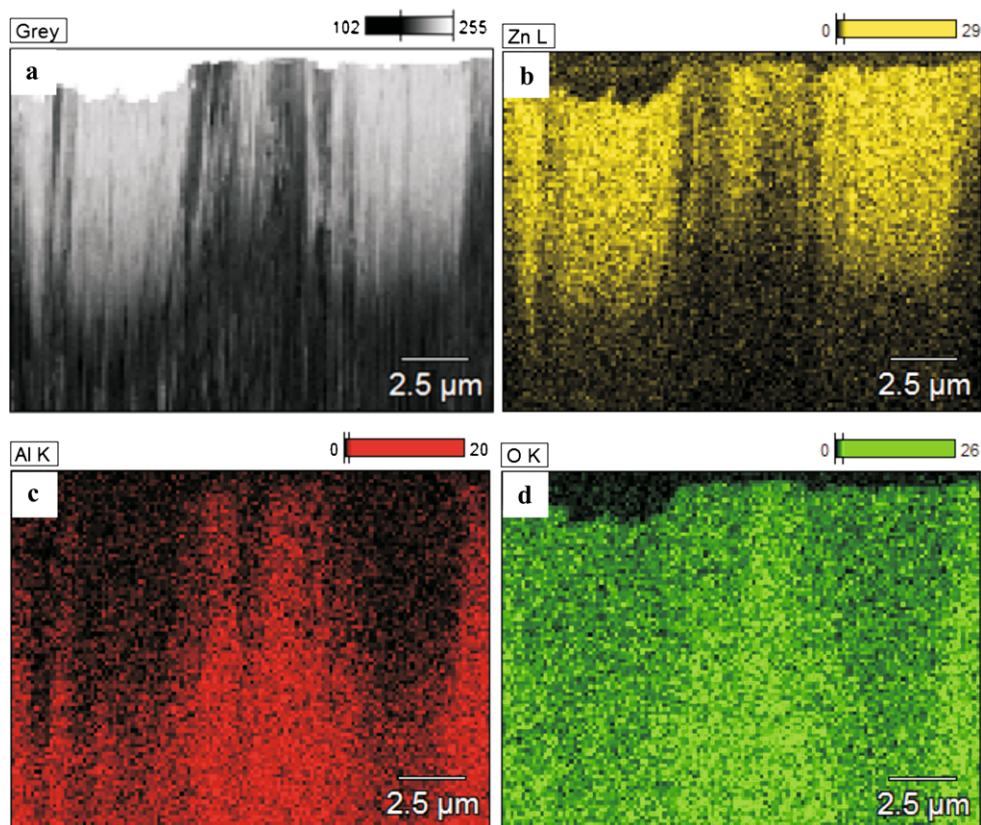


Fig. 2 EDS spectra of sample 1' (a) and sample 2' (b)

Fig. 3 BSE micrograph (a) and EDS elemental maps of Zn (L-line) (b), Al (K-line) (c), and O (K-line) (d) of sample 1



graphs of selected parts of the sample cut by FIB. Figure 4a shows the sample in the bright field (BF) image mode in which a heavier ZnO phase exhibits a dark and the lighter Al_2O_3 phase light contrast, respectively. Figure 4b shows the same part of the sample in the STEM Z-contrast mode (obtained using HAADF detector) clearly showing bright ZnO nanorods embedded into a darker Al_2O_3 template. The entire ZnO/AAO material forms a sort of a nanocomposite. Figure 4c shows the selected area electron diffraction

(SAED) pattern taken from the ZnO. Bright rings in the SAED are corresponding to (100), (002), (101), (102), (2–10), (103), and (2–12) planes of polycrystalline ZnO. This confirms that the ZnO nanorods have hexagonal wurtzite structure.

Figure 5 displays the PL spectra and decay profiles of ZnO nanorods before and after their covering with Ag nanoparticles. Both samples of the 1st and 2nd type exhibit a broad blue PL emission, as previously observed for ZnO

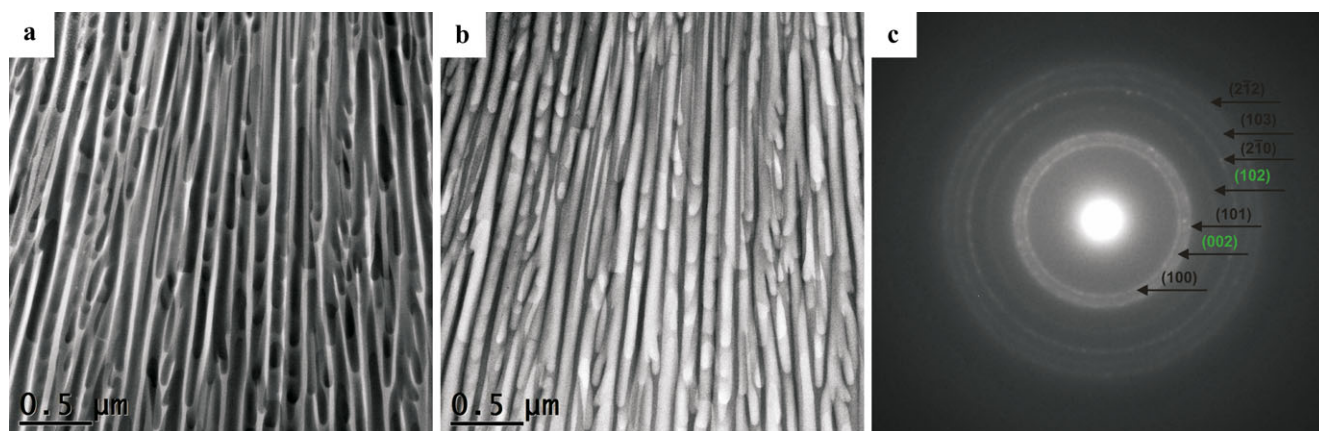


Fig. 4 STEM images showing the microstructure of the ZnO/AAO composite material: BF (a) and Z-contrast (HAADF detector) (b); SAED pattern of ZnO in the interior of the AAO nanopores (c)

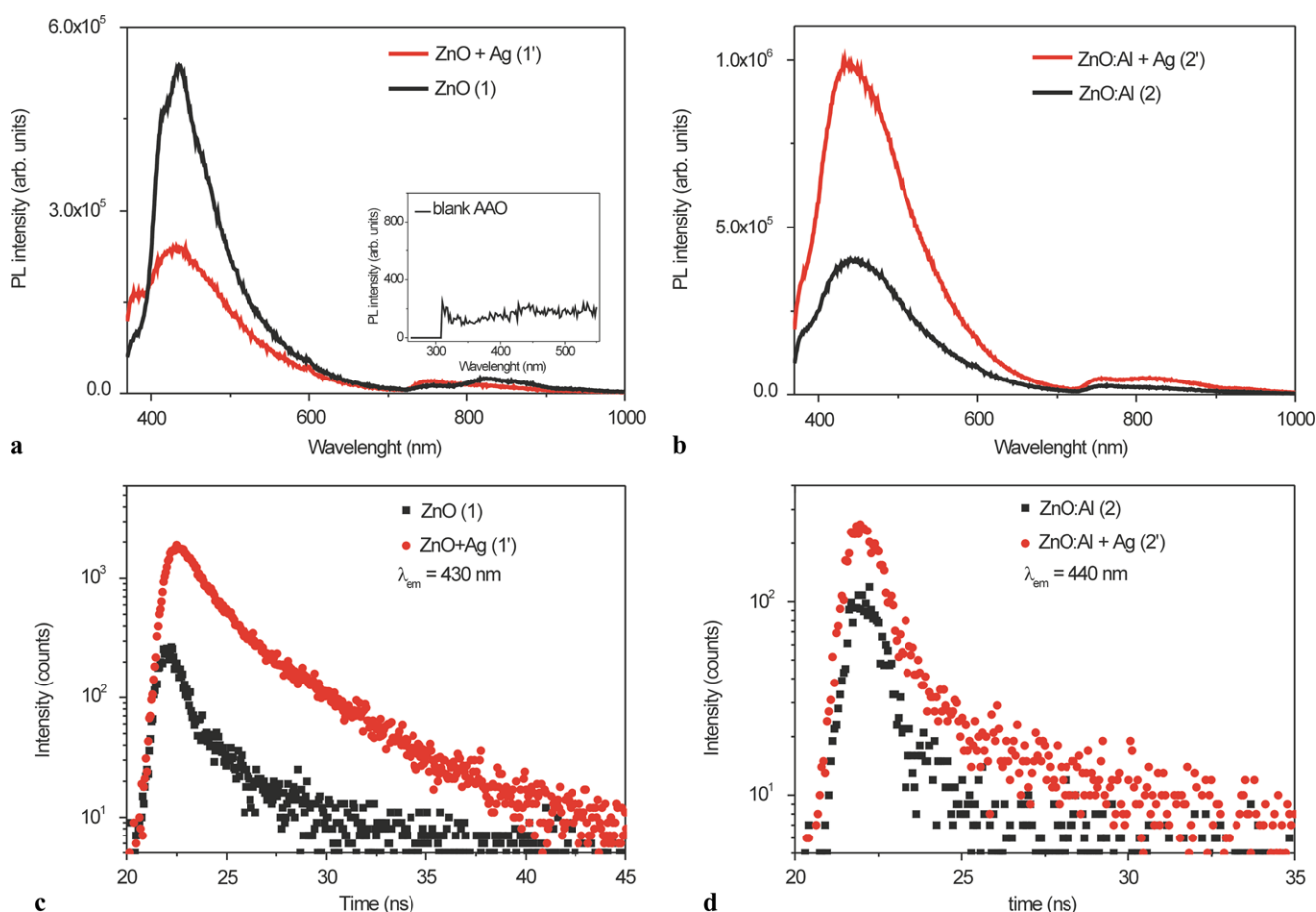


Fig. 5 PL spectra of samples 1 and 1' (a) and samples 2 and 2' (b) (in the inset: PL spectra of blank AAO); decay profiles of blue band in samples 1 and 1' (c) and samples 2 and 2' (d)

nanoparticles embedded in the AAO [18, 19]. The strong ultraviolet emission, expected for high-quality and undoped wurtzite ZnO structures, is missing in the spectra indicating a poor crystal quality of ZnO synthesized on the AAO. The blue PL emission at about 2.84 eV (436 nm) was attributed

to the recombination of carriers trapped at Zn_i (electrons) and V_{Zn} (holes) [11]. Such identification of the PL band was based on the results of modeling by the full potential linear muffin-tin orbital method, which estimated position of the V_{Zn} level at 3.06 eV below the conduction band and

the position of the Zn_i level at 0.22 eV below the conduction band [3].

Deposition of Ag nanoparticles enhances the PL intensity only for the 2nd-type samples. There the PL intensity is enhanced by about 2.5 times. Various reasons can be responsible for this behavior. It might be that the coupling between the Ag plasmons and the ZnO DAPs is different in two types of the samples. This may relate the difference in their morphology. The nanostructures of the 2nd type are characterized by higher disorder giving rise to higher surface-to-volume ratio of a whole material. Thus, the PL enhancement may be due to larger interfacial contact area between Ag and ZnO and, consequently, the enhanced interaction between them. In samples of the first type, the contact area is smaller. Then, some nonradiative channels might have been activated, resulting in the suppression of the luminescence. Since the maximum surface plasmon resonance (SPR) occurs at 400–460 nm in Ag nanoparticles of the size between 10–20 nm [29], the visible light emitted from the ZnO nanocrystals can be considerably absorbed by the Ag nanoparticles, leading to the quenching of the ZnO emission. This apparently holds for sample 1'. However, due to the larger interfacial contact area between Ag nanoparticles and ZnO surface in sample 2', the excited electrons in the Ag nanoparticles can easily transfer to the conduction band of ZnO. Because the conduction band of ZnO is higher than the Fermi level of Ag (Fig. 5, Ref. [20]) these electrons are without difficulty transferred back to the Fermi level of Ag, which is higher than the defect level located at ZnO. Due to the similar energy values between the Fermi level of Ag and the defect level in ZnO, there is another efficient energy transfer from Ag Fermi level to the defect level at the ZnO side, and the DAP emission is enhanced in the case of sample 2'.

There are other possibilities. For instance, electrons at defect levels of ZnO could be excited via energy transfer from Ag. In this case no holes are trapped at acceptor levels, and thus DAP emission is not observed. Finally, the efficiency of plasmonic effect can be affected by the dimension of nanostructures and of the Ag nanoparticles. In samples of the second-type Ag particles are finer than in samples of the second type (Figs. 1c and 1f).

The decay times of the blue PL were studied to elucidate PL enhancement mechanism. They are in nanoseconds range as previously observed [30]. The decay time τ_d increases in sample 1' as compared to sample 1 (from 2.3 ns to 4.1 ns) and remains nearly stable in case of samples 2 and 2' (1.9 ns and 2.2 ns, respectively). A change of the observed decay time of fluorescence, $\tau_d = 1/(k_f + k_{nr})$, is fairly small. It can reflect changes of the rates of either the radiative, k_f , or nonradiative, k_{nr} , processes, or both of them [31].

PL enhancement effects by plasmonic effect were observed in several cases (see, e.g., Ref. [32]). There the prox-

imity of emitting centers (about 10 nm) to silver islands resulted in increased emission intensities and decreased lifetimes. In the present case, a decreased PL lifetime is not observed. Thus, the higher emission intensity can result from light scattering by silver NPs. The PL enhancement may be due to excitation of the dipolar SP of the silver NPs. Then the electro-magnetic field of excited SP can increase the transition probabilities of the nanorods absorption resulting in the increase intensity of emission with tiny increase of the emission lifetime.

4 Conclusions

Luminescent properties of ZnO nanorods covered with Ag nanoparticles are examined. The ZnO nanorods were deposited using AAO templates with the ALD technique. Two types of the samples were prepared with different arrangement of ZnO nanorods. Both types of samples exhibit a broad emission centered at around 440 nm most probably originating from zinc interstitial (Zn_i) defects. The blue emission was further altered by the Ag nanoparticles depositions. The sample with a random distribution of ZnO nanorods and finer Ag nanoparticles demonstrates the luminescence enhancement by factor of ~ 2.5 upon Ag deposition, whereas samples with regular arrangement of ZnO nanorods show the luminescence suppression. The material can be interesting from the point of view of its application in blue range emitting diodes.

Acknowledgements The work has been financially supported by the European Union within European Regional Development Fund through grant Innovative Economy (POIG.01.01.02-00-008/08) and by the Polish Ministry of Science and Higher Education, Project LAPROMAW (POIG.02.01.00-14-071/08/00). Thanks are due to Prof. Jerzy Bystrzycki, Military University of Technology, Poland, for his help in arranging the HR TEM measurements.

Open Access This article is distributed under the terms of the Creative Commons Attribution License which permits any use, distribution, and reproduction in any medium, provided the original author(s) and the source are credited.

References

1. A.B.M.A. Ashrafi, A. Ueta, A. Avramescu, H. Kumano, I. Suenmune, *Appl. Phys. Lett.* **76**, 550 (2000)
2. H. Morkoç, Ü. Özgür, *Zinc Oxide: Fundamentals, Materials and Device Technology* (Wiley-VCH, Weinheim, 2009)
3. C.H. Ahn, Y.Y. Kim, D.C. Kim, S.K. Mohanta, H.K. Cho, *J. Appl. Phys.* **105**, 013502 (2009)
4. A. Janotti, C.G. van de Walle, *Phys. Rev. B* **76**, 165202 (2007)
5. D. Haranath, S. Sahai, P. Joshi, *Appl. Phys. Lett.* **92**, 233113 (2008)
6. G. Luka, T.A. Krajewski, B.S. Witkowski, G. Wisz, I.S. Virt, E. Guziewicz, M. Godlewski, *J. Mater. Sci., Mater. Electron.* **22**, 1810 (2011)

7. S. Grzanka, G. Łuka, T.A. Krajewski, E. Guziewicz, R. Jachymek, W. Purgal, R. Wiśniewska, A. Sarzyńska, A. Bering-Staniszevska, M. Godlewski, P. Perlin, *Acta Phys. Pol. A* **119**, 672 (2011)
8. S. Lin Ye Z, H. He, B. Zhao, L. Zhu, J. Huang, *J. Appl. Phys.* **104**, 064311 (2008)
9. J.D. Ye, S.L. Gu, F. Qin, S.M. Zhu, S.M. Liu, X. Zhou, W. Liu, L.Q. Hu, R. Zhang, Y. Shi, Y.D. Zheng, *Appl. Phys. A* **81**, 759 (2005)
10. J. Zhao, L. Qin, Y. Zhang, Y. Hao, Q. Guo, L. Zhang, *Micro Nano Lett.* **5**, 336 (2010)
11. K.H. Tam, C.K. Cheung, Y.H. Leung, A.B. Djuricic, C.C. Ling, C.D. Beling, S. Fung, W.M. Kwok, W.K. Chan, D.L. Phillips, L. Ding, W.K. Ge, *J. Phys. Chem. B* **110**, 20865 (2006)
12. Z. Wang, H.L. Li, *Appl. Phys. A* **74**, 201 (2002)
13. N. Kumar, G.D. Varma, R. Nath, A.K. Srivastava, *Appl. Phys. A* **104**, 1169 (2011)
14. S. Öztürk, N. Taştun, N. Kılınç, H. Yüzer, Z.Z. Öztürk, *Appl. Phys. A* **99**, 73 (2010)
15. C.J. Yang, S.M. Wang, S.W. Liang, Y.H. Chang, C. Chen, J.M. Shieh, *Appl. Phys. Lett.* **90**, 033104 (2007)
16. M.J. Zheng, L.D. Zhang, G.H. Li, W.Z. Shen, *Chem. Phys. Lett.* **363**, 123 (2002)
17. M. Wu, L. Yao, W. Cai, G. Jiang, X. Li, Z. Yao, *J. Mater. Sci. Technol.* **20**, 11 (2004)
18. Z. Fang, Y. Wang, X. Peng, X. Liu, C. Zhen, *Mater. Lett.* **57**, 4187 (2003)
19. H. Zhang, X. Li, G. Hu, Y. Li, *J. Mater. Sci., Mater. Electron.* **21**, 950 (2010)
20. X.D. Zhou, X.H. Xiao, J.X. Xu, G.X. Cai, F. Ren, C.Z. Jiang, *Europhys. Lett.* **93**, 57009 (2011)
21. Y. Harada, I. Tanahashi, N. Ohno, *J. Lumin.* **129**, 1759 (2009)
22. H. Lu, X. Xu, L. Lu, M. Gong, Y. Liu, *J. Phys. Condens. Matter* **20**, 472202 (2008)
23. M.K. Lee, T.G. Kim, W. Kim, Y.M. Sung, *J. Phys. Chem. C* **112**, 10079 (2008)
24. B.J. Lawrie, R.F. Haglund, R. Mu, *Opt. Express* **17**, 2565 (2009)
25. J. Xie, Q. Wu, *Mater. Lett.* **64**, 389 (2010)
26. C. Karunakaran, V. Rajeswari, P. Gomithisankar, *Solid State Sci.* **13**, 923 (2011)
27. C. Karunakaran, V. Rajeswari, P. Gomithisankar, *J. Alloys Compd.* **508**, 587 (2010)
28. G. Łuka, L. Wachnicki, B.S. Witkowski, T.A. Krajewski, R. Jakiela, E. Guziewicz, M. Godlewski, *Mater. Sci. Eng. B* **176**, 237 (2011)
29. K.-C. Lee, S.-J. Lin, C.-H. Lin, Ch.-S. Tsai, Y.-J. Lu, *Surf. Coat. Technol.* **202**, 5339 (2008)
30. J.M. Azpiroz, E. Mosconi, F. de Angelis, *J. Phys. Chem. C* **115**, 25219 (2011)
31. M. Norek, J. Dresner, J. Prochorow, *Acta Phys. Pol. A* **104**, 425 (2003)
32. J.R. Lakowicz, *Anal. Biochem.* **337**, 171 (2005)